

Linearly polarized gluons at next-to-next-to leading order and the Higgs transverse momentum distribution

Daniel Gutierrez-Reyes,^a Sergio Leal-Gomez,^{a,b} Ignazio Scimemi,^a Alexey Vladimirov^c

^a*Departamento de Física Teórica and IPARCOS, Universidad Complutense de Madrid (UCM), 28040 Madrid, Spain*

^b*University of Vienna, Faculty of Physics, Boltzmannngasse 5, A-1090 Wien, Austria*

^c*Institut für Theoretische Physik, Universität Regensburg, D-93040 Regensburg, Germany*

E-mail: dangut01@ucm.es, sergiol95@univie.ac.at, ignazios@ucm.es,
alexey.vladimirov@ur.de

ABSTRACT: We calculate the small- b (or large- q_T) matching of transverse momentum dependent (TMD) distribution for linearly polarized gluons to the integrated gluon distributions at the next-to-next-to-leading order (NNLO). This is the last missing part for the complete NNLO prediction of the Higgs spectrum within TMD factorization. We discuss the numerical impact of the correction so derived to the q_T -differential cross-section for Higgs boson production and to the positivity bound for linearly polarized gluon transverse momentum distribution.

Contents

1	Introduction	1
2	Gluon TMD distributions	2
2.1	Definition	2
2.2	OPE at small- b	3
2.3	Renormalization of TMDPDF	4
3	Matching coefficient for lpTMDPDF at NNLO	6
3.1	Evaluation of matching coefficient	6
3.2	Logarithmic part of the coefficient function	8
3.3	Finite part of coefficient function	9
4	lpTMDPDF at NNLO and its contribution Higgs production	9
5	Conclusions	12
A	Relevant set of master integrals for linearly polarized gluon TMD	13
B	Logarithm terms of matching coefficient for lpTMDPDF	15

1 Introduction

The gluon-gluon fusion is the leading channel for the Higgs boson production in hadron-hadron collisions [1–3]. The transverse momentum dependent (TMD) factorization of Higgs production has been demonstrated to follow the same pattern as the Drell-Yan/vector boson case [4–7] and in this sense it has been reviewed in [8]. Within the TMD factorization theorem, which describes the Higgs production at small transverse momentum, there are two dominant terms in the factorized cross-section. Those terms correspond to the fusion of unpolarized and the linearly polarized gluons [9–11]. Schematically, it reads

$$\frac{d\sigma}{dydq_T} = \frac{\sigma_{gg\rightarrow H}}{(2\pi)^2} \int d\mathbf{b} e^{-i(\mathbf{b}q_T)} \left(f_{1,g}(x_A, \mathbf{b}) f_{1,g}(x_B, \mathbf{b}) + h_{1,g}^\perp(x_A, \mathbf{b}) h_{1,g}^\perp(x_B, \mathbf{b}) \right), \quad (1.1)$$

where $\sigma_{gg\rightarrow H}$ is the factorized gluon-gluon-Higgs cross-section, $x_{A,B}$ are the collinear fractions of gluon momenta, f_1 is the unpolarized gluon transverse momentum dependent parton distribution function (TMDPDF) and $h_{1,g}^\perp$ is the linearly polarized gluon TMDPDF (lpTMDPDF) that was proposed as an independent distribution a long ago by Mulders and Rodrigues [12].

The TMD factorization approach considers each TMD distribution ($f_{1,g}$ and $h_{1,g}^\perp$ in this case) as an independent fundamental function that is, generally, of non-perturbative origin. In particular kinematic regimes, TMD distributions can be asymptotically merged to other observables. The most important case is the small- b limit, where the TMD distributions match to collinear parton distributions and the matching coefficient is calculable in QCD perturbation theory [4, 5, 13]. This interpretation is the main difference of the TMD factorization from the resummation approach that is intensively used in high-energy physics, see e.g. [11, 14–18], where the small- b expansion

is incorporated into the factorization formula, ignoring the non-perturbative TMD effects. Therefore, the TMD factorization is equivalent to the resummation approach for large enough q_T . The consequence of this difference in interpretations is different requirements in the realization of the perturbative series. So, while in the resummation approach the whole bracketed factor in eq. (1.1) should be of a given order, in the TMD factorization approach each distribution should be matched to its collinear counterpart at the same given order. Typically this difference is unimportant, and both approaches are consistent with computing the small- b expansion at the same order. In the case of linearly polarized gluon contribution to eq. (1.1), the counting is, however, different, because the tree-order contribution to lpTMDPDF vanishes.

The modern state-of-the-art of perturbative calculations is the next-to-next-to-leading order (NNLO) of perturbative series, see [19–21]. Such a high order is required to match the sizes of theoretical and experimental uncertainties, see e.g., [18, 22]. Also, it is required for the use of NNLO TMD evolution, which is necessary to perform an accurate global analysis of high- and low-energy data [23, 24]. The small- b limit of the unpolarized gluon TMDPDF, f_1 , has been calculated at NNLO in [19, 20]. However the small- b limit of the lpTMDPDF, $h_{1,g}^\perp$ is known only at one-loop [8, 11, 21] and as such it has been used in ref. [25]. In this work, we fill this gap, providing the calculation of $h_{1,g}^\perp$ at two loops and estimating the impact of this correction on the Higgs transverse momentum spectrum. The calculation can be performed using the same techniques as in ref. [20, 26–28].

The result obtained in this work is relevant for many cases beyond the Higgs boson production. In particular, there are processes that are also sensitive to lpTMDPDF and that are addressed in the literature [29–33]. Among these it is worth a special mentioning the case of heavy-quark production [34–38], which is relevant at LHC, future Electron-Ion Collider (EIC) or the LHeC. Another important topic is the positivity bound for gluon TMDPDF derived in [12],

$$|h_{1,g\leftarrow h}^\perp(x, \mathbf{q}_T)|/|f_{1,g\leftarrow h}(x, \mathbf{q}_T)| \leq 1. \quad (1.2)$$

This positivity bound is expected to saturate at small- x due to the McLerran-Venugopalan model [39]. Our calculation shows that this bound is easily violated by loop corrections but could be restored by non-perturbative corrections. In this way, the relation in eq. (1.2) could be considered as a strong restriction on transverse momentum dependence of partons.

The two-loop calculation presented here is structured in a way similar to the case of unpolarized gluons, evaluated in [20]. We find it sufficient to recall the basic principles and notation in sec. 2, which can be skipped by the reader already acquainted with topical works. The computation has requested the calculations of several new master integrals which are reported in the appendix. The final result for the NNLO matching of $h_{1,g}^\perp$ onto collinear gluon PDF is presented in sec. 3. The presented NNLO matching has been incorporated into `artemide` [40], which was used to perform a qualitative numerical estimation of lpTMDPDF to Higgs-production cross-section at NNLO-N³LL. The results of the phenomenological analysis are discussed in sec. 4.

2 Gluon TMD distributions

2.1 Definition

The TMD distribution of gluons in a hadron is given by the following matrix element

$$\begin{aligned} \Phi_{g\leftarrow h,\mu\nu}(x, \mathbf{b}) &= \frac{1}{xp^+} \int \frac{d\lambda}{2\pi} e^{-i\lambda p^+} \\ &\times \langle P, S | \bar{T} \left\{ F_{+\mu}(\lambda n + \mathbf{b}) \tilde{W}_n(\lambda n + \mathbf{b}) \right\} T \left\{ \tilde{W}_n^\dagger(0) F_{+\nu}(0) \right\} | P, S \rangle, \end{aligned} \quad (2.1)$$

where n is a lightlike vector, $F^{\mu\nu}$ is the gluon field strength tensor, and \tilde{W} denotes the half-infinite Wilson line in the direction n

$$\tilde{W}_n(z) = P \exp \left(ig \int_{-\infty}^0 d\sigma A_+(n\sigma + z) \right). \quad (2.2)$$

The Wilson lines \tilde{W}_n are taken in the adjoint representation of the gauge group. We use the standard notation for the lightcone components of vector $v^\mu = n^\mu v^- + \bar{n}^\mu v^+ + g_T^{\mu\nu} v_\nu$ (with $n^2 = \bar{n}^2 = 0$, $n \cdot \bar{n} = 1$, and $g_T^{\mu\nu} = g_{\mu\nu} - n^\mu \bar{n}^\nu - \bar{n}^\mu n^\nu$).

The decomposition of the gluon TMD distribution over independent Lorenz structures contains 8 components [8, 12]. Two of these structures survive in the case of unpolarized hadron

$$\Phi_{g\leftarrow h}^{\mu\nu}(x, \mathbf{b}) = -\frac{g_T^{\mu\nu}}{2(1-\epsilon)} f_{1,g\leftarrow h}(x, \mathbf{b}) + h_{1,g\leftarrow h}^\perp(x, \mathbf{b}) \left(\frac{g_T^{\mu\nu}}{2(1-\epsilon)} + \frac{b^\mu b^\nu}{\mathbf{b}^2} \right), \quad (2.3)$$

where $\mathbf{b}^2 = -b^2 > 0$. For future necessity, the decomposition in eq. (2.3) is given in $d = 4 - 2\epsilon$ -dimensions as it was defined in [19, 21]. Both f_1 and h_1^\perp contribute to the gluon-induced TMD processes on equal foot. Although these functions share some common properties, they are completely independent non-perturbative functions that are to be extracted from the experiment.

The usage of a d -dimensional definition for the decomposition in eq. (2.3) is important for the following two-loop calculation because the ϵ -dependent parts influence the result. The definition in eq. (2.3) is the standard one [19, 21] written such that the unpolarized part coincides with the standard definition of the unpolarized TMDPDF, see e.g. [4, 19, 20] (here dots denote the staple gauge link, as in (2.1)),

$$f_{1,g\leftarrow h}(x, \mathbf{b}) = -g_T^{\mu\nu} \Phi_{g\leftarrow h, \mu\nu}(x, \mathbf{b}) = \frac{1}{xp^+} \int \frac{d\lambda}{2\pi} e^{-i\lambda p^+} \langle P | F_{+\mu}(\lambda n + \mathbf{b}) \dots F_{+\mu}(0) | P \rangle, \quad (2.4)$$

whereas the linearly-polarized tensor is orthogonal to it. In turn the lpTMDPDF is given by

$$h_{1,g\leftarrow h}^\perp(x, \mathbf{b}) = \frac{1}{1-2\epsilon} \left(g_T^{\mu\nu} + 2(1-\epsilon) \frac{b^\mu b^\nu}{\mathbf{b}^2} \right) \Phi_{g\leftarrow h, \mu\nu}(x, \mathbf{b}). \quad (2.5)$$

Sometimes, one would like to use TMD distributions defined in the momentum space. The relation between coordinate and momentum representation is the usual one [8, 12] (here in $d = 4$ dimensions),

$$\begin{aligned} \Phi_{g\leftarrow h, \mu\nu}(x, \mathbf{k}) &= \int \frac{d^2\mathbf{b}}{(2\pi)^2} e^{i(\mathbf{b}\mathbf{k})} \Phi_{g\leftarrow h, \mu\nu}(x, \mathbf{b}) \\ &= -\frac{g_T^{\mu\nu}}{2} f_{1,g\leftarrow h}(x, \mathbf{k}) + h_{1,g\leftarrow h}^\perp(x, \mathbf{k}) \left(\frac{g_T^{\mu\nu}}{2} + \frac{k^\mu k^\nu}{\mathbf{k}^2} \right), \end{aligned} \quad (2.6)$$

where

$$f_{1,g\leftarrow h}(x, \mathbf{k}) = \int_0^\infty \frac{|\mathbf{b}|d|\mathbf{b}|}{2\pi} J_0(|\mathbf{b}||\mathbf{k}|) f_{1,g\leftarrow h}(x, \mathbf{b}), \quad (2.7)$$

$$h_{1,g\leftarrow h}^\perp(x, \mathbf{k}) = -\int_0^\infty \frac{|\mathbf{b}|d|\mathbf{b}|}{2\pi} J_2(|\mathbf{b}||\mathbf{k}|) h_{1,g\leftarrow h}^\perp(x, \mathbf{b}). \quad (2.8)$$

2.2 OPE at small- b

At small- b the TMD operator can be matched to the collinear operators by means of operator product expansion (OPE). This relation is important because it constrains the model for TMD distributions at small values of b . Moreover, at large values of Q , where the TMD evolution

factor significantly suppress the large- b part of the Fourier integral, the small- b OPE provides the dominating input to the cross-section (see e.g. [8, 11, 25] for studies related to Higgs boson processes).

The systematic description of the small- b OPE applied to TMD operators can be found in ref. [41]. In the present case, it results into the following expressions

$$f_{1,g\leftarrow h}(x, \mathbf{b}; \mu, \zeta) = \sum_f \int_x^1 \frac{dy}{y} C_{g\leftarrow f}(y, \mathbf{b}; \mu, \zeta; \tilde{\mu}) f_{1,f\leftarrow h}\left(\frac{x}{y}, \tilde{\mu}\right) + \mathcal{O}(\mathbf{b}^2) \quad (2.9)$$

$$h_{1,g\leftarrow h}^\perp(x, \mathbf{b}; \mu, \zeta) = \sum_f \int_x^1 \frac{dy}{y} \delta^L C_{g\leftarrow f}(y, \mathbf{b}; \mu, \zeta; \tilde{\mu}) f_{1,f\leftarrow h}\left(\frac{x}{y}, \tilde{\mu}\right) + \mathcal{O}(\mathbf{b}^2), \quad (2.10)$$

where the sum runs over the active parton flavors (quarks and gluon), and $f_1(x, \mu)$ is unpolarized collinear distributions defined as usual

$$f_{1,q\leftarrow h}(x, \mu) = \int \frac{d\lambda}{2\pi} e^{-ixp^+\lambda} \langle P | \bar{T} \{ \bar{q}(\lambda n) \tilde{W}_n(\lambda n) \} \frac{\gamma^+}{2} T \{ \tilde{W}_n^\dagger(0) q(0) \} | P \rangle, \quad (2.11)$$

$$f_{1,g\leftarrow h}(x, \mu) = \frac{1}{xp^+} \int \frac{d\lambda}{2\pi} e^{-ixp^+\lambda} \langle P | \bar{T} \{ F_{+\mu}(\lambda n) \tilde{W}_n(\lambda n) \} T \{ \tilde{W}_n^\dagger(0) F_{+\mu}(0) \} | P \rangle. \quad (2.12)$$

Concerning the notation, here and in the following we distinguish the unpolarized TMDPDF $f_1(x, \mathbf{b})$ and unpolarized collinear PDF $f_1(x)$ by the number of arguments. The scales μ and ζ in eq. (2.9, 2.10) are the scales of TMD evolution discussed in the next section. The scale $\tilde{\mu}$ is the scale of OPE, that is not related to the TMD evolution scales and whose dependence cancels in the convolution of coefficient function and collinear distribution.

The coefficient functions (also known as matching coefficients [4]), C and $\delta^L C$, are to be calculated in QCD perturbation theory. The three-order calculation yields

$$C_{g\leftarrow f}(x, \mathbf{b}; \mu, \zeta; \tilde{\mu}) = \delta_{gf} \delta(1-x) + \mathcal{O}(a_s), \quad (2.13)$$

$$\delta^L C_{g\leftarrow f}(x, \mathbf{b}; \mu, \zeta; \tilde{\mu}) = \mathcal{O}(a_s), \quad (2.14)$$

where $a_s = g^2/(4\pi)^2$ is QCD coupling constant. Nowadays, the coefficients $C_{f\leftarrow h}(x, \mathbf{b})$ are known at a_s^2 -order (NNLO) [19, 20, 26, 42], whereas coefficients $\delta^L C_{f\leftarrow h}(x, \mathbf{b})$ are known at a_s -order (NLO¹) [8, 11, 21]. In the following section we present NNLO expression for $\delta^L C_{g\leftarrow f}$, which allows to consider these distributions at the same level of accuracy.

The corrections to the OPE at higher powers of b are unknown but at large value of \mathbf{b}^2 the OPE becomes divergent. Thus, in practice, for the description of the TMD distributions one typically uses a phenomenological ansatz that matches the OPE results at small- b to a non-perturbative input at large- b . It can be written in the form

$$h_{1,g\leftarrow h}^\perp(x, \mathbf{b}) = \sum_f \int_x^1 \frac{dy}{y} \delta^L C_{g\leftarrow f}(y, \mathbf{b}) f_{1,f\leftarrow h}\left(\frac{x}{y}\right) f_{\text{NP}}(x, y, \mathbf{b}^2), \quad (2.15)$$

and similar for $f_1(x, \mathbf{b})$. In eq. (2.15) we omit scale variables, and the function f_{NP} is an arbitrary function with the only constraint

$$\lim_{\mathbf{b}^2 \rightarrow 0} f_{\text{NP}}(x, y, \mathbf{b}^2) \simeq 1 + \mathcal{O}(\mathbf{b}^2). \quad (2.16)$$

2.3 Renormalization of TMDPDF

The TMD operator contains ultraviolet (UV) and rapidity divergences. Both these divergences can be renormalized (the all-order proof of renormalization for rapidity divergences is given in ref. [7])

¹In literature related to TMD calculations, e.g. in refs. [8, 21], the orders of $\delta^L C_{f\leftarrow h}$ are traditionally counted alike the unpolarized case. So, the a_s -term that are formally LO, denoted as NLO. We use the same convention.

by the corresponding renormalization factors. Hence, the renormalized (or physical) TMD distribution depends on two scales μ (the UV renormalization scale) and ζ (the rapidity divergences renormalization scale). The renormalized expression for the TMD distribution $\Phi_{g\leftarrow h}$ reads

$$\Phi_{g\leftarrow h}(x, \mathbf{b}; \mu, \zeta) = Z_g^{\text{TMD}}(\mu, \zeta|\epsilon) R_g \left(\mathbf{b}, \mu, \zeta | \epsilon, \frac{\delta^+}{p^+} \right) \Phi_{g\leftarrow h}^{\text{unsub.}} \left(x, \mathbf{b} | \epsilon, \frac{\delta^+}{p^+} \right), \quad (2.17)$$

where $\Phi_{g\leftarrow h}^{\mu\nu; \text{unsub.}}$ denotes the bare or unsubtracted TMD distribution, either f_1 either h_1^\perp , since the TMD renormalization is independent of polarization properties. In eq. (2.17) we present explicitly the dependence on regularization parameters: ϵ is the parameter of dimensional regularization ($d = 4 - 2\epsilon$) that regularizes UV divergences, that are renormalized by the factor Z_g ; δ is the parameter of δ -regularization [20, 27] which regularizes rapidity divergences that are renormalized by the factor R_g . The renormalization factors Z_g and R_g are ordered such that the renormalization of rapidity divergences is made before to the renormalization of UV divergences as it was done in similar NNLO calculations [20, 26, 28]. The final result is independent of the subtraction order.

The rapidity renormalization factor can be related to the TMD soft factor [7], which is the vacuum expectation value of certain Wilson loop [4, 5, 7],

$$S(\mathbf{b}) = \frac{\text{Tr}_{\text{color}}}{N_c} \langle 0 | [W_n^{T\dagger} \tilde{W}_{\bar{n}}^T] (\mathbf{b}) [\tilde{W}_{\bar{n}}^{T\dagger} W_n^T] (0) | 0 \rangle, \quad (2.18)$$

where \tilde{W}_n and $\tilde{W}_{\bar{n}}$ are Wilson lines along n and \bar{n} (2.2). In the case of gluon operators the Wilson loop is in the adjoint representation. The rapidity divergences are regularized by the δ -regularization, which consists in suppression of the gluon field in a Wilson line by exponential factor, $A_+(n\sigma + x) \rightarrow A_+(n\sigma + x)e^{-\delta|\sigma|}$. The rapidity divergences reveals as $\ln(\delta)$. In this scheme the rapidity renormalization factor is [7, 27, 43]

$$R_g \left(\mathbf{b}, \mu, \zeta | \epsilon, \frac{\delta^+}{p^+} \right) = S^{-1/2} \left(\mathbf{b} | \epsilon, \delta = \frac{\delta^+}{2p^+} \sqrt{\zeta} \right). \quad (2.19)$$

The variable p^+ is parton momentum [41], and is required to define the Lorentz invariant scale ζ . Note, that the definition (2.19) also contains finite at $\delta \rightarrow 0$ terms, which can be seen as a scheme-dependence. Commonly, the scheme dependence is fixed by condition that no remnants of the soft factor appear in the hard part of the factorization theorem [4, 7]. Definition (2.19) satisfies this condition. The UV renormalization factor is taken in $\overline{\text{MS}}$ -scheme.

The (μ, ζ) -dependence of gluon TMD distribution is provided by a pair of evolution equations

$$\mu^2 \frac{d}{d\mu^2} \Phi_{g\leftarrow h}(x, \mathbf{b}; \mu, \zeta) = \frac{\gamma^g(\mu, \zeta)}{2} \Phi_{g\leftarrow h}(x, \mathbf{b}; \mu, \zeta), \quad (2.20)$$

$$\zeta \frac{d}{d\zeta} \Phi_{g\leftarrow h}(x, \mathbf{b}; \mu, \zeta) = -\mathcal{D}_g(\mu, \mathbf{b}) \Phi_{g\leftarrow h}(x, \mathbf{b}; \mu, \zeta). \quad (2.21)$$

These equations are the same for all gluon TMD distributions of leading twist. The anomalous dimensions are defined via the corresponding renormalization constants and they are known up to three-loop order inclusively [44–47]. Note, that the renormalization factor Z_g also contains the gluon-field renormalization part, therefore,

$$\gamma_G = 2\widehat{AD}(Z_3 - Z_g) \quad (2.22)$$

where the symbol \widehat{AD} extracts the coefficient of ϵ^{-1} with a pre-factor $n!$ at the n^{th} perturbative order.

Anomalous dimensions γ^g and \mathcal{D} satisfy the integrability condition (also known as Collins-Soper equation [48])

$$2\mu^2 \frac{d\mathcal{D}_g(\mathbf{b}, \mu)}{d\mu^2} = -\zeta \frac{d\gamma^g(\mu, \zeta)}{d\zeta} = \Gamma_{\text{cusp}}^g(\mu), \quad (2.23)$$

where Γ_{cusp} is anomalous dimension for cusp of two light-like Wilson lines (in the adjoint representation). Due to this equation the expression for γ^g can be rewritten in the form

$$\gamma^g(\mu, \zeta) = \Gamma_{\text{cusp}}^g(\mu) \ln \left(\frac{\mu^2}{\zeta} \right) - \gamma_V^g, \quad (2.24)$$

where γ_V^g is anomalous dimension of the vector form factor for gluon. The rapidity anomalous dimension \mathcal{D}_g has not such a simple representation due to the presence of an extra dimensional parameter \mathbf{b}^2 . It generally contains all powers of logarithms $\ln(\mu^2 \mathbf{b}^2)$, that at some large values of \mathbf{b}^2 turns to some non-perturbative function [49].

Due to the integrability condition in eq. (2.23) the system of evolution equations in eq. (2.20, 2.21) has a unique solution:

$$\Phi_{g \leftarrow h}(x, \mathbf{b}; \mu_1, \zeta_1) = R^g[\mathbf{b}; (\mu_1, \zeta_1) \rightarrow (\mu_2, \zeta_2)] \Phi_{g \leftarrow h}(x, \mathbf{b}; \mu_2, \zeta_2), \quad (2.25)$$

where the TMD renormalization factor reads

$$R^g[\mathbf{b}; (\mu_1, \zeta_1) \rightarrow (\mu_2, \zeta_2)] = \exp \left[\int_P \left(\gamma^g(\mu, \zeta) \frac{d\mu}{\mu} - \mathcal{D}_g(\mu, \mathbf{b}) \frac{d\zeta}{\zeta} \right) \right]. \quad (2.26)$$

Here, P is arbitrary path in (μ, ζ) -plane connecting (μ_1, ζ_1) and (μ_2, ζ_2) . The eq. (2.26) is in principle independent of the path P , however the truncation of the perturbative series makes some choices more preferable, for the detailed discussion see ref. [22]. In particular, in sec. 4 we use the special practically-convenient path that corresponds to ζ -prescription introduced in [22, 23]. We again stress that the TMD evolution equations and their solution of eq. (2.25) do not depend on the polarization, and thus it is exactly same for unpolarized TMDPDF f_1 and lpTMDPDF h_1^\perp .

3 Matching coefficient for lpTMDPDF at NNLO

3.1 Evaluation of matching coefficient

The coefficient function for OPE at twist-2 level can be deduced from the calculation of matrix elements with free parton states with subsequent matching of the result on the desired OPE structures eq. (2.10). Therefore, the task is naturally split into two steps: the evaluation of parton-matrix element and the matching. This procedure is well-known, see e.g. [4, 5, 8, 20, 26, 28], in this section we present only minimal details and specifics of calculation of lpTMDPDF.

The evaluation of parton matrix elements of the TMD operators at two-loop level is the most complicated part of the present work. We have used the same technique that was used by our group for NNLO evaluations in refs. [8, 20, 28], where we refer for extra details. In the case of lpTMDPDF the main complication comes from the rich vector structure, which is reduced to scalar products by projection factor in eq. (2.5), and the use of unpolarized parton states with momentum $p^\mu = p^+ n^\mu$. In this aspect the current computation is similar to evaluation of the pretzelosity distribution [28] albeit with significantly larger number of loop-integrals. The reduction of integrals to master integrals and some details of their evaluation is presented in the appendix A.

The outcome of each diagram at NNLO has a generic form

$$\begin{aligned} \text{diag.} = (\mathbf{b}^2)^{2\epsilon} & \left(g_1(x, \epsilon) + \left(\frac{\delta^+}{p^+} \right)^\epsilon g_2(x, \epsilon) + \left(\frac{\delta^+}{p^+} \right)^{-\epsilon} g_3(x, \epsilon) \right. \\ & \left. + \ln \left(\frac{\delta^+}{p^+} \right) g_4(x, \epsilon) + \ln^2 \left(\frac{\delta^+}{p^+} \right) g_5(x, \epsilon) \right). \end{aligned} \quad (3.1)$$

The functions g_2 and g_3 exactly cancel in the sum of all the diagrams (and this fact can be also traced in the sum of sub-classes of diagrams) because they represent IR divergences. The last two

terms represent the rapidity diverging pieces, and thus the functions g_4 and g_5 are canceled by the rapidity renormalization factor. However, due to the absence of three-order term, the functions g_5 cancel in the diagrams. The cancellation of all these pieces provides a check of the calculation.

Summing together the diagrams we obtain the un-subtracted expression for TMDPDF on free-gluon states. Let us introduce the notation for perturbative series

$$h_{1,f\leftarrow f'}^{\perp;\text{unsub.}}(x, \mathbf{b}) = \Phi_{f\leftarrow f'}^{\text{unsub.}}(x, \mathbf{b}) = \sum_{n=1}^{\infty} a_s^n \Phi_{f\leftarrow f'}^{[n]\text{unsub.}}, \quad S(\mathbf{b}) = 1 + \sum_{n=1}^{\infty} a_s^n S^{[n]}, \quad (3.2)$$

where $a_s = g^2/(4\pi)^2$. The tree-order term is zero in the case of lpTMDPDF,

$$\Phi_{f\leftarrow f'}^{[0]\text{unsub.}} = 0, \quad (3.3)$$

which provides many simplifications. In this notation, the expression for the renormalized lpTMDPDF in eq. (2.17) on a parton reads

$$\Phi_{f\leftarrow f'}^{[1]} = \Phi_{f\leftarrow f'}^{[1]\text{unsub.}} \quad (3.4)$$

$$\Phi_{f\leftarrow f'}^{[2]} = \Phi_{f\leftarrow f'}^{[2]\text{unsub.}} - \frac{S^{[1]}\Phi_{f\leftarrow f'}^{[1]\text{unsub.}}}{2} + Z_g^{[1]\text{TMD}}\Phi_{f\leftarrow f'}^{[1]\text{unsub.}}. \quad (3.5)$$

The expressions for Z_g^{TMD} is given in ref. citeEchevarria:2016scs, while the expression for the soft factor in δ -regularization is in ref. [27].

Given the values of parton matrix elements we find the coefficient functions matching left- and right-hand sides of

$$h_{1,g\leftarrow f}^{\perp}(x, \mathbf{b}) = \sum_{f=g,q,\bar{q}} [\delta^L C_{g\leftarrow f}(\mathbf{b}) \otimes f_{1,f'\leftarrow f}(x)], \quad (3.6)$$

where $f_{1,f'\leftarrow f}$ is the renormalized parton matrix element for PDF operator eq. (2.11), and \otimes is the short-hand notation for Mellin convolution integral eq. (2.10). Such a relation is valid since the OPE is an operator relation and it is independent of states.

To solve the matching in eq. (3.6) we need the expression for the collinear matrix elements $f_{1,f'\leftarrow f}$. This calculation is trivial in the actual scheme since there is no Lorenz-invariant scale inside the integrands and all loop-integrals for $f_{1,f'\leftarrow f}$ are zero in dimensional regularization. For this reason the loop-corrections to $f_{1,f'\leftarrow f}$ are given by UV renormalization constant only:

$$f_{1,f\leftarrow f'}^{[0]}(x) = \delta_{ff'}\delta(1-x), \quad f_{1,f\leftarrow f'}^{[1]}(x) = -\frac{P_{f\leftarrow f'}^{[1]}(x)}{\epsilon}, \quad (3.7)$$

where $P^{[1]}$ is the DGLAP evolution kernel at LO.

Denoting the perturbative terms for the matching coefficient as

$$\delta^L C_{g\leftarrow f}(x, \mathbf{b}) = \sum_{n=1}^{\infty} a_s^n \delta^L C_{g\leftarrow f}^{[n]}(x, \mathbf{b}), \quad (3.8)$$

we find from eq. (3.6, 3.7),

$$\delta^L C_{g\leftarrow f}^{[0]}(x, \mathbf{b}) = 0, \quad \delta^L C_{g\leftarrow f}^{[1]}(x, \mathbf{b}) = h_{g\leftarrow f}^{\perp[1]}(x, \mathbf{b}), \quad (3.9)$$

$$\delta^L C_{g\leftarrow f}^{[2]}(x, \mathbf{b}) = h_{g\leftarrow f}^{\perp[2]}(x, \mathbf{b}) + \frac{1}{\epsilon} \sum_{f'} [\delta^L C_{g\leftarrow f'}^{[1]}(\mathbf{b}) \otimes P_{f'\leftarrow f}^{[1]}(x)]. \quad (3.10)$$

This procedure cancels the collinear poles that are present in the parton matrix elements. Note that, the last term in eq. (3.10) requires the evaluation of $\delta^L C^{[1]}$ to order $\sim \epsilon$.

3.2 Logarithmic part of the coefficient function

The renormalization group equation allows us to write down the coefficients that accompany the scaling logarithms in the coefficient function. We recall that the coefficient function depends on three scales see eq. (2.10): μ and ζ that are inherited from the TMDPDF, and $\tilde{\mu}$ that is the scale of OPE. The behavior on scales μ and ζ is dictated by the TMD evolution equations (2.20, 2.21), while the dependence on scale $\tilde{\mu}$ is canceled by the corresponding dependence of $f_1(x, \tilde{\mu})$. The latter is given by the DGLAP equation

$$\mu^2 \frac{d}{d\mu^2} f_{1,f \leftarrow h}(x, \mu) = \sum_{f'=g,q,\bar{q}} \int_x^1 \frac{dy}{y} P_{f \leftarrow f'}\left(\frac{x}{y}, \mu\right) f_{1,f' \leftarrow h}(y, \mu), \quad (3.11)$$

Therefore, at the point $\mu = \tilde{\mu}$ the coefficient function satisfies the pair of equations

$$\mu^2 \frac{d}{d\mu^2} \delta^L C_{g \leftarrow f}(x, \mathbf{b}; \mu, \zeta, \mu) \quad (3.12)$$

$$= \sum_{f'=g,q,\bar{q}} \int_x^1 \frac{dy}{y} \delta^L C_{g \leftarrow f'}\left(\frac{x}{y}, \mathbf{b}; \mu, \zeta, \mu\right) \left(\frac{\gamma_V^g(\mu, \zeta)}{2} \delta_{ff'} \delta(\bar{y}) - P_{f' \leftarrow f}(y, \mu) \right),$$

$$\zeta \frac{d}{d\zeta} \delta^L C_{g \leftarrow f}(x, \mathbf{b}; \mu, \zeta, \mu) = -\mathcal{D}_g(\mu, \mathbf{b}) \delta^L C_{g \leftarrow f}(x, \mathbf{b}; \mu, \zeta, \mu). \quad (3.13)$$

The solution at NNLO has the simple form

$$\delta^L C_{g \leftarrow f}^{[2]}(x, \mathbf{b}; \mu, \zeta, \mu) = \left(-\frac{1}{2} \mathbf{L}_\mu^2 + \mathbf{L}_\mu \mathbf{l}_\zeta \right) \delta^L C_{g \leftarrow f}^{(2,1,1)}(x) + \mathbf{L}_\mu \delta^L C_{g \leftarrow f}^{(2,1,0)}(x) + \delta^L C_{g \leftarrow f}^{(2,0,0)}(x), \quad (3.14)$$

where

$$\mathbf{L}_\mu = \ln \left(\frac{\mu^2 \mathbf{b}^2}{4e^{-\gamma_E}} \right), \quad \mathbf{l}_\zeta = \ln \left(\frac{\mu^2}{\zeta} \right). \quad (3.15)$$

The coefficients of logarithms are

$$\delta^L C_{g \leftarrow f}^{(2,1,1)}(x) = \frac{\Gamma_0^g}{2} \delta^L C_{g \leftarrow f}^{(1,0,0)}(x), \quad (3.16)$$

$$\delta^L C_{g \leftarrow f}^{(2,1,0)}(x) = 2\beta_0 \delta^L C_{g \leftarrow f}^{(1,0,0)}(x) - \sum_{f'=g,q,\bar{q}} [\delta^L C_{g \leftarrow f'}^{(1,0,0)} \otimes P_{f' \leftarrow f}^{[1]}](x),$$

where $\Gamma_0^g = 4C_A$ is LO cusp anomalous dimension, $\beta_0 = 11/3C_A - 2/3N_f$ is LO β -function, and we have used that $\gamma_V^{g[1]} = -2\beta_0$. The explicit expressions for these coefficients are given in the appendix B for completeness. The finite parts $\delta^L C^{(n;0,0)}$ are presented in the next section.

In the expressions above we have set $\tilde{\mu} = \mu$, which is a poor choice. In particular, due to this choice one obtains the double-logarithms in the coefficient function and, as the result, a badly convergent perturbative series. A much better behaved coefficient function can be achieved by distinguishing the scales of evolution and OPE. For example, this is realized by applying the ζ -prescription, which consists in the selection of TMD evolution scales along the null-evolution line in the plane (μ, ζ) . This line is parameterized as $\zeta = \zeta_\mu(\mathbf{b})$, and it is defined by the boundary condition that it passes through the saddle point of the evolution potential [22]. The expression for the coefficient function can be obtained by the substitution (here for gluon distributions)

$$\text{in } \zeta\text{-prescription:} \quad \mathbf{l}_\zeta = \frac{\mathbf{L}_\mu}{2} - \frac{2\beta_0}{\Gamma_0^g} + \mathcal{O}(a_s). \quad (3.17)$$

The higher order terms and the derivation of this expression can be found in ref. [22, 23]. The coefficient function in ζ -prescription satisfies DGLAP equation, and thus the remaining scale is the OPE scale $\tilde{\mu}$. In other words, we have

$$\delta^L C_{g \leftarrow f}(x, \mathbf{b}; \mu, \zeta_\mu(b), \tilde{\mu}) = \delta^L C_{g \leftarrow f}(x, \mathbf{b}; \tilde{\mu}), \quad (3.18)$$

where the logarithmic part has simple form

$$\delta^L C_{g \leftarrow f}^{[2]}(x, \mathbf{b}; \tilde{\mu}) = \left(\beta_0 \delta^L C_{g \leftarrow f}^{(1,0,0)}(x) - \sum_{f'=g,q,\bar{q}} [\delta^L C_{g \leftarrow f'}^{(1,0,0)} \otimes P_{f' \leftarrow f}^{[1]}](x) \right) \mathbf{L}_{\tilde{\mu}} + \delta^L C_{g \leftarrow f}^{(2,0,0)}(x). \quad (3.19)$$

The finite part $\delta^L C_{g \leftarrow f}^{(2,0,0)}(x)$ remains unaffected. Note that, generally the ζ -prescription also modifies the finite part of NNLO expression, as it happens e.g. for the unpolarized TMDPDF.

3.3 Finite part of coefficient function

In this section we present the finite parts of coefficient function $\delta^L C$. The NLO expression read

$$\delta^L C_{g \leftarrow g}^{(1,0,0)}(x, \mathbf{b}) = -C_A \frac{4(1-x)}{x}, \quad (3.20)$$

$$\delta^L C_{g \leftarrow q}^{(1,0,0)}(x, \mathbf{b}) = -C_F \frac{4(1-x)}{x}, \quad (3.21)$$

where $C_A = N_c (= 3)$ and $C_F = (N_c^2 - 1)/2N_c (= 4/3)$ are eigenvalues of quadratic Casimir operators for adjoint and fundamental representations in $SU(N_c)$ ($SU(3)$) group. The result in eq. (3.20, 3.21) agrees with [8, 11, 21]. The full ϵ -dependent NLO expressions are presented in [21]. The NNLO expressions are

$$\begin{aligned} \delta^L C_{g \leftarrow g}^{(2;0,0)}(x) &= C_A^2 \left\{ 16 \frac{1-x}{x} \left[\frac{55}{36} + \frac{5}{4} \zeta_2 + \ln x - \text{Li}_2(x) - 2\text{Li}_3(1-x) \right] \right. \\ &\quad + \frac{x(x+3)}{4} \left[\frac{31}{9} - \zeta_2 - \zeta_3 + \ln x + 2\text{Li}_2(1-x) - \ln x \text{Li}_2(x^2) + \text{Li}_3(x^2) \right] \\ &\quad + \frac{x+3}{4} \left[41 + 2 \ln x \ln(1-x) + 2 \ln x \ln(1+x) + \text{Li}_2(x^2) \right] - \frac{388}{9} + \frac{124}{3} \ln x - 8 \ln^2 x \left. \right\} \\ &\quad + C_F N_f \cdot 4 \left[\ln^2 x - 2 \frac{(1-x)^3}{x} \right] + C_A N_f \cdot \frac{4}{9} \left[17 \frac{1-x}{x} + 1 - 3x - x^2 + 6 \ln x \right], \\ \delta^L C_{g \leftarrow q}^{(2;0,0)}(x) &= C_F (C_F - C_A) \left[8 \frac{1-x}{x} (\ln(1-x) + \ln^2(1-x)) - 20 \ln x + 4 \ln^2 x + 8(1-x) \right] \\ &\quad + C_F C_A \left[16 \frac{1-x}{x} \left(\frac{11}{18} + \frac{5}{4} \zeta_2 + \ln x - \frac{\ln(1-x)}{3} - \text{Li}_2(x) - 2\text{Li}_3(1-x) \right) \right. \\ &\quad \left. + 36 \ln x - 4 \ln^2 x \right] + C_F N_f \cdot \frac{16}{9} \frac{1-x}{x} (2 + 3 \ln(1-x)), \end{aligned} \quad (3.22)$$

where N_f is the number of active quark flavors. These expressions is the main result of this work.

4 lpTMDPDF at NNLO and its contribution Higgs production

In general, the lpTMDPDF appears in the same processes as the unpolarized gluon TMDPDF. A particularly important place to study the effect of lpTMDPDF is the Higgs production in hadron-hadron collision. In this case the dominating channel for Higgs production is gluon-gluon fusion via the top-quark loop [1], which can be written via an effective interaction term in the Lagrangian [50]

$$\mathcal{L}_{ggH} = \frac{a_s(\mu) C_t(\mu)}{3v} F_{\mu\nu}^A F^{A,\mu\nu} H, \quad (4.1)$$

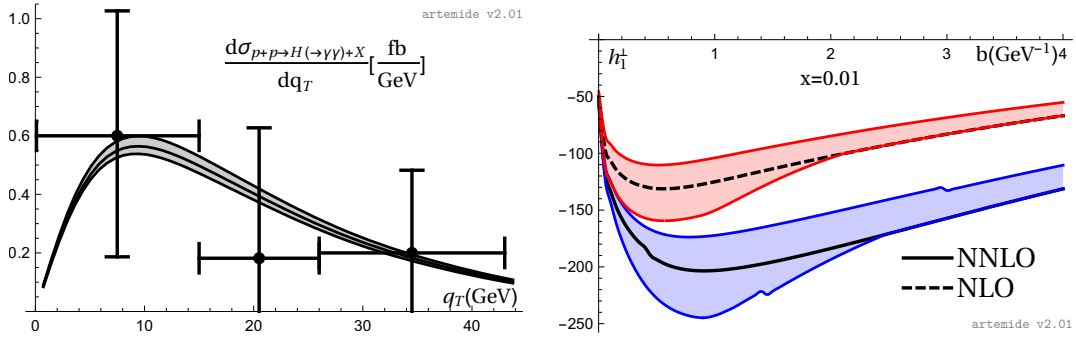


Figure 1. (left) Comparison of Higgs-production cross-section with variation band to the measurement presented in [55] by CMS collaboration. (right) The lpTMDPDF as a function of \mathbf{b} at $x = 0.01$. The shaded area shows the variation band in $\tilde{\mu}$.

where H is the Higgs field, $F_{\mu\nu}$ is the gluon field strength tensor, and v is the Higgs vacuum expectation value. The effective coupling constant at NNLO is derived in [51, 52]. Using the effective vertex in eq. (4.1) one can derive the TMD factorization theorem for Higgs production following the same steps as in the Drell-Yan case (see e.g. ref. [53]). The resulting expression is

$$\frac{d\sigma}{dyd^2\mathbf{q}_T} = \frac{2\sigma_0(\mu)}{\pi} C_t^2(\mu) U(\mu, -\mu) |C_H(-m_H^2, -\mu^2)|^2 \int \frac{d^2\mathbf{b}}{4\pi} e^{i(\mathbf{b}\mathbf{q}_T)} \Phi_{g\leftarrow h_1}^{\mu\nu}(x_1, \mathbf{b}; \mu, \zeta_1) \Phi_{g\leftarrow h_2}^{\mu\nu}(x_2, \mathbf{b}; \mu, \zeta_2), \quad (4.2)$$

where y is the Higgs rapidity and $x_{1,2} = \sqrt{(m_H^2 + \mathbf{q}_T^2)}/se^{\pm y}$. The function C_H is the gluon scalar form-factor (the NNLO expression can be found in [45]), U is the “ π^2 -resummation” exponent [54] and the TMD distributions $\Phi^{\mu\nu}$ are defined in eq. (2.1). For a more accurate and detailed definition we refer to ref. [53]. The scale μ is of the order of the hard scale, m_H in this case, and $\zeta_1\zeta_2 = m_H^4$.

With the decomposition in eq. (2.3) the product of TMD distributions turns into

$$\Phi_{g\leftarrow h_1}^{\mu\nu}(x_1, \mathbf{b}) \Phi_{g\leftarrow h_2}^{\mu\nu}(x_2, \mathbf{b}) = \frac{1}{2} (f_{1,g\leftarrow h_1}(x_1, \mathbf{b}) f_{1,g\leftarrow h_2}(x_2, \mathbf{b}) + h_{1,g\leftarrow h_1}^\perp(x_1, \mathbf{b}) h_{1,g\leftarrow h_2}^\perp(x_2, \mathbf{b})). \quad (4.3)$$

Therefore, for a consistent phenomenological application of this formula one should consider f_1 and h_1^\perp at the same perturbative order. It is interesting to mention that if the Higgs boson would be a pseudo-scalar particle, then the main change in the structure of cross-section in eq. (4.2) would be a sign of $h_1^\perp h_1^\perp$ term in eq. (4.3). In this case, the expressions for perturbative corrections in C_t and C_H are also changed although their LO remains the same [10].

In order to study the numerical impact of our result, the NLO and NNLO matching for lpTMDPDF together with the cross-section in eq. (4.2) have been added to `artemide` [40]. The non-perturbative parts of gluon TMD distributions and gluon rapidity anomalous dimension are unknown, and nowadays the data is not sufficient to fix it (see fig. 1(left), for comparison of the theory and experimental precisions). Therefore, we have used the following assumptions. The non-perturbative functions f_{NP} in eq. (2.15) have been taken the same for both f_1 and h_1^\perp with the same values as it was extracted in the quark case in [23] (with unpolarized collinear gluon PDF taken from NNPDF3.1 set [56]). It should give a reasonable estimation for the sizes of non-perturbative effects, while the main numerical difference comes from the values of matching coefficients. The rapidity anomalous dimension is taken the same as in extracted [24] with additional rescaling by factor C_A/C_F (Casimir scaling).

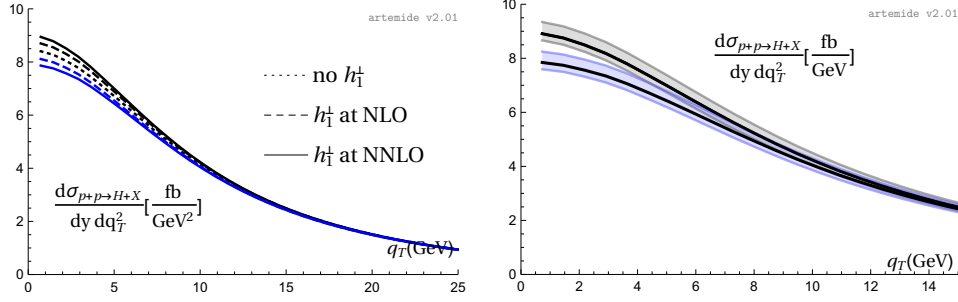


Figure 2. Cross section for Higgs production including linearly polarized gluon effects at different orders. The blue lines correspond to the negative contribution for $h_1^\perp h_1^\perp$ -term in (4.3), which roughly simulates a parity odd Higgs particle. (left) The motion of center lines of cross-section at different perturbative orders for lpTMDPDF. (right) The scale-variation band for the cross section at NNLO.

Since the tree level matching of the lpTMDPDF is null, and the actual LO is $\sim a_s^1$, lpTMDPDF is expected to receive a relatively large correction at order a_s^2 . This fact is confirmed in fig. 1(right). The difference between NLO and NNLO is practically of order 2 at $x = 0.01$. The bands show the sensitivity of the distribution to the change of the OPE scale $\tilde{\mu} \rightarrow c_4 \tilde{\mu}$ with $c_4 \in (0.5, 2)$. The relative size of the band decreases between NLO and NNLO, although not essentially. Altogether, this figure points to the fact that the lpTMDPDF effects could have been underestimated up to now. In the Higgs production cross-section lpTMDPDF mainly affects the low- q_T region, as it is demonstrated in fig. 2. Practically, the lpTMDPDF can be distinguished from the unpolarized TMDPDF at $q_T \lesssim 5 - 8\text{GeV}$, where it modifies the values of cross-section by about 5%. Such value of variation band is typical for NNLO approximation, see e.g. [18]. In fig. 2(right) we also demonstrate the size of the variation band, which is the maximum deviation value obtained from the variation of all three scales (in ζ -prescription) by factors $c_i \in (0.5, 2)$ [22]. The variation band is of the order of few percents and the main contribution to it is the μ -band (the scale between hard part and the TMD-evolution factor). Nowadays, these factors can be pushed to N³LO reducing the variation band further, if necessary.

Finally, we comment on the positivity relation formulated in ref. [12]:

$$|f_1(x, \mathbf{q}_T)| - |h_1^\perp(x, \mathbf{q}_T)| > 0. \quad (4.4)$$

This relation is a consequence of positive definiteness of the gluon-polarization matrix in a free theory, and certainly holds at LO. However, it does not need to be accomplished at higher order in perturbation theory. The positivity bound is formulated in momentum space, whereas all perturbative calculations are performed in coordinate space. This causes an additional problem since the Hankel transform of a positive function is not necessarily a positive function. Within our model we have checked that it is easy to get a violation of this bound, for any fixed value of x and q_T . Typically, the violation happens in the vicinity of the sing-change point of f_1 (note, that our realization of f_1 is positive-definite in \mathbf{b} -space). Outside of this point the inequality in eq. (4.4) is respected. The situation is exemplified in fig. 3, where we plot the ratio of $|f_1|/|h_1^\perp|$ at different values of q_T with fixed x (left) and viceversa (right). We also note that the positions of zeros in TMDPDFs strongly depend on the non-perturbative input. In particular, selecting some appropriate model one can, possibly, remove the zero from unpolarized TMDPDF, or fix positions of zeros equal in both gluon TMDPDFs. In other words eq. (4.4) can be used as a serious constraint on the non-perturbative part of the TMD distributions. However, we do not see enough theoretical justification for such an approach at the moment.

We have also observed that the ratio $|h_1^\perp|/|f_1|$ tends to saturate at smaller values of x as it is

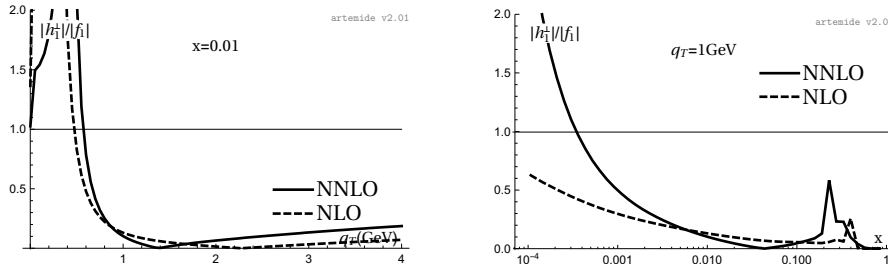


Figure 3. Ratio of linearly polarized and unpolarized gTMD to check as in eq. (1.2) as a function of q_T at $x = 0.01$ (left) and as a function of x at $q_T = 1$ (right).

suggested f.i. by [39]. Then for extreme small values of $x \sim 10^{-4}$ it is violated again. However, such values can be outside the applicability region of our calculation since the perturbative expressions for f_1 [20] and h_1^\perp (3.22, 3.23) have contributions $\sim a_s^{n+1} \ln^n(x)/x$ that should be resummed for a proper comparison.

5 Conclusions

The gluon transverse momentum dependent parton distribution function (lpTMDPDF) typically accompanies unpolarized gluon TMDPDF within a TMD factorized cross-section. A good example is the factorization formula for the Higgs-production cross-section, where these distributions enter in a plain sum. For this reason, both distributions should be considered at the same order of perturbative accuracy. We have calculated the a_s^2 -part (NNLO) for the matching coefficient of lpTMDPDF to twist-2 collinear distributions, which is the main result of this paper. Thanks to this calculation, lpTMDPDF can be considered at the same level of theoretical accuracy as the unpolarized gluon TMDPDF [19, 20]. The corresponding formulas are collected in sec.3.2, 3.3. They are also attached to the publication in the form of *Mathematica*-notebook. The module for the numerical evaluation of lpTMDPDF is added to the *artemide* package that can be downloaded from [40].

The impact of NNLO correction for lpTMDPDF is very significant and practically doubles the value of the function for moderate b . This fact should not be considered much surprising given that LO term (a_s^0 -term) for lpTMDPDF vanishes. The relevance of this effect in the Higgs cross section has been discussed in sec. 4 and it is resummed in figs. 1-2. Unfortunately, at the moment we have not a reliable model for the non-perturbative part of the gluon TMD distribution, and in this work, we have adapted values for distributions extracted in refs. [23, 24]. A more detailed study on the non-perturbative part of the gluon TMDPDF is certainly worth in the future.

In several papers, it has been suggested that unpolarized and linearly polarized gluon TMDPDFs can be measured in association with heavy-quark production [34–38]. We leave an analysis of these processes for future work because at the moment we miss a full factorization theorem for these cases. Nevertheless, the consistency of data with the factorization hypothesis can always be checked with the result provided in this work.

Acknowledgements

D.G.R., S.L.G. and I.S. are supported by the Spanish MECD grant FPA2016-75654-C2-2-P. This project has received funding from the European Union Horizon 2020 research and innovation program under grant agreement No 824093 (STRONG-2020). D.G.R. acknowledges the support of the Universidad Complutense de Madrid through the predoctoral grant CT17/17-CT18/17. S.L.G. is

supported by the Austrian Science Fund FWF under the Doctoral Program W1252-N27 Particles and Interactions.

A Relevant set of master integrals for linearly polarized gluon TMD

Three different types of diagrams arise in the calculation of the unsubtracted TMDPDF matrix element for linearly polarized gluons and they can be addressed on the basis that the exchanged gluons are pure-virtual, virtual-real or real-real. The pure-virtual diagrams, are zero in the dimensional regularization due to the absence of a Lorentz-invariant scale in our scheme of calculation. The virtual-real and real-real diagrams have respectively one and two cut propagators and should be computed directly. The calculation of these two types of diagrams is analogous to the calculation made in ref. [20, 26] for the case of unpolarized TMDPDF, albeit with a different Lorentz structure. The main difference and difficulty comes from the term proportional to $b^\mu b^\nu$. The contraction of this term with the projectors generates terms in the numerator as $(\mathbf{b}\mathbf{q})^2$ (where \mathbf{q} is a loop-momentum), making the evaluation of the diagrams involved.

For virtual-real diagrams this difficulty can be by-passed by calculating separately virtual sub-diagrams. This approach allows to contract the projector only with the real loop-momentum, simplifying the calculation of integrals. For real-real integrals no subdiagrams can be calculated. A set of master integrals in which these diagrams can be decomposed was developed in [20]. In this appendix we present the decomposition of the master integrals original for this work.

A general master integral can be written as

$$F_{abcd}[R] = (2\pi)^2 \int \frac{d^{d-1}k d^{d-1}l}{(2\pi)^{2d}} \frac{R e^{i(\mathbf{k}\mathbf{b})} e^{i(\mathbf{l}\mathbf{b})} \delta(k^2) \theta(-k^-) \delta(l^2) \theta(-l^-)}{[(l+p)^2]^a [(k+p)^2]^b [(k+l+p)^2]^c [(k+l)^2]^d}, \quad (\text{A.1})$$

where $R = \{1, (\mathbf{k}\mathbf{b})^2, (\mathbf{k}\mathbf{b})(\mathbf{l}\mathbf{b}), (\mathbf{l}\mathbf{b})^2\}$. The bold font denotes the scalar product of transverse components only with Euclidian metric. The components k^+ and l^+ can be integrated with the help of the introduction of a delta function

$$1 = \int_{-\infty}^{\infty} d\eta p^+ \delta((1-\eta)p^+ + l^+) \quad (\text{A.2})$$

and they do not enter in the loop-integration (indicated by a $d-1$ integral).

The integrals with $R = 1$, $F_{abcd}[1] \equiv F_{abcd}$ are presented in the Appendix C of [20]. In that case, the sum of the indices $abcd$ of the integral is 2. In the present calculation, the new integrals with $R \neq 1$ and the sum of the indices $abcd$ is 3. Some of the new integrals can be expressed as a

combination of older results,

$$F_{0210}[(\mathbf{k}\mathbf{b})^2]/\mathbf{B} = 2 \left((1+2\epsilon)(x-\eta) - \frac{\epsilon(1-2\epsilon)}{1+\epsilon} \frac{1-\eta}{x} \right) F_{0110} - \frac{2(1-2\epsilon)}{1+\epsilon} (1-x)F_{0020}, \quad (\text{A.3})$$

$$F_{0210}[(\mathbf{k}\mathbf{b})(\mathbf{l}\mathbf{b})]/\mathbf{B} = \frac{2(1-2\epsilon)}{1+\epsilon} \frac{1-\eta}{1+x-\eta} \left(\epsilon \frac{1-\eta}{x} F_{0110} - (1+\epsilon)(\eta-x)F_{0110} + (1-x)F_{0020} \right) + 2(1+x-\eta)F_{(-1)210} + 2\eta F_{0110}, \quad (\text{A.4})$$

$$F_{0210}[(\mathbf{l}\mathbf{b})^2]/\mathbf{B} = \frac{x}{(1+x-\eta)^2} \left(\frac{2(1-2\epsilon)}{1+\epsilon} (x(\eta-x) - (1+\epsilon)(1-\eta)) F_{0110} + \epsilon \frac{2(1-2\epsilon)}{1+\epsilon} x(1-x)F_{0020} - 2(1-2\epsilon)(1-\eta)^2 F_{0110} \right) - 4(1-\eta)F_{(-1)210} - \frac{1}{(1+x-\eta)^2} \left(\frac{2\epsilon(1-2\epsilon)}{1+\epsilon} \frac{(1-\eta)^3}{x} - 2\eta(1-2\epsilon)(1-\eta)^2 \right) F_{0110} - \frac{2(1-2\epsilon)}{1+\epsilon} \frac{(1-\eta)^2}{(1+x-\eta)^2} (1-x)F_{0020}, \quad (\text{A.5})$$

$$F_{0120}[(\mathbf{k}\mathbf{b})^2]/\mathbf{B} = \left(4(x-\eta) + \frac{2(1-2\epsilon)}{1+\epsilon} \frac{1-x}{x} (1+x-\eta) \right) F_{0020} + \epsilon \frac{2(1-2\epsilon)}{1+\epsilon} \frac{1-\eta}{x^2} (1+x-\eta) F_{0110}, \quad (\text{A.6})$$

$$F_{0120}[(\mathbf{k}\mathbf{b})(\mathbf{l}\mathbf{b})]/\mathbf{B} = -\frac{2(1-2\epsilon)}{1+\epsilon} \frac{1-\eta}{x} \left(\epsilon \frac{1-\eta}{x} F_{0110} + (1-x)F_{0020} \right) - 2F_{0110} + 2(1+x-\eta)F_{(-1)210} + 2\eta F_{0020}, \quad (\text{A.7})$$

$$F_{0120}[(\mathbf{l}\mathbf{b})^2]/\mathbf{B} = \frac{2(1-2\epsilon)}{1+\epsilon} \frac{(1-\eta)^2}{x(1+x-\eta)} \left(\epsilon \frac{1-\eta}{x} F_{0110} + (1+\epsilon) \frac{x}{1-\eta} F_{0110} + (1-x)F_{0020} \right) - 4(1-\eta)F_{(-1)210}, \quad (\text{A.8})$$

$$F_{1020}[(\mathbf{k}\mathbf{b})^2]/\mathbf{B} = \frac{2(1-2\epsilon)}{1+\epsilon} \frac{(\eta-x)^2}{x\eta} \left(\epsilon \frac{\eta-x}{x} F_{1010} + (1+\epsilon) \frac{x}{\eta-x} F_{1010} + (1-x)F_{0020} \right) + 4(x-\eta)F_{1(-1)20}, \quad (\text{A.9})$$

$$F_{1020}[(\mathbf{k}\mathbf{b})(\mathbf{l}\mathbf{b})]/\mathbf{B} = -\frac{2(1-2\epsilon)}{1+\epsilon} \frac{\eta-x}{x} \left(\epsilon \frac{\eta-x}{x} F_{1010} + (1-x)F_{0020} \right) - 2F_{1010} + 2(1+x-\eta)F_{0020} + 2\eta F_{1(-1)20}, \quad (\text{A.10})$$

$$F_{1020}[(\mathbf{l}\mathbf{b})^2]/\mathbf{B} = \frac{2(1-2\epsilon)}{1+\epsilon} \frac{\eta}{x} \left(\epsilon \frac{\eta-x}{x} F_{1010} + (1-x)F_{0020} \right) - 4(1-\eta)F_{0020}, \quad (\text{A.11})$$

$$F_{0021}[(\mathbf{k}\mathbf{b})^2]/\mathbf{B} = -\frac{2(1-2\epsilon)}{1-\epsilon} \frac{\eta-x}{1-x} ((1+x-\eta)F_{0020} - (\eta-x)F_{0011}) + 4(x-\eta) (F_{0011} - F_{0020} - F_{(-1)021}), \quad (\text{A.12})$$

$$F_{0021}[(\mathbf{k}\mathbf{b})(\mathbf{l}\mathbf{b})]/\mathbf{B} = \frac{2(1-2\epsilon)}{1-\epsilon} \frac{(\eta-x)(1-\eta)}{1-x} (F_{0020} + F_{0011}) + 2(1+x-2\eta)F_{(-1)021} - 2(1-\eta) (F_{0011} - F_{0020}) - 2F_{0020}, \quad (\text{A.13})$$

$$F_{0021}[(\mathbf{l}\mathbf{b})^2]/\mathbf{B} = -\frac{2(1-2\epsilon)}{1-\epsilon} \frac{1-\eta}{1-x} (\eta F_{0020} - (1-\eta)F_{0011}) - 4(1-\eta)F_{(-1)021}, \quad (\text{A.14})$$

where $\mathbf{B} = \mathbf{b}^2/4$.

Additionally, we have met three integrals that could not be reduced to a combination of known results: $F_{1110}[(\mathbf{k}\mathbf{b})^2]$, $F_{1110}[(\mathbf{k}\mathbf{b})(\mathbf{l}\mathbf{b})]$, $F_{1110}[(\mathbf{l}\mathbf{b})^2]$. For these integrals we have derived the expressions in the Schwinger parameterization, and evaluated them in ϵ -expansion up to the finite term following the strategy described in the book [57].

B Logarithm terms of matching coefficient for lpTMDPDF

In this appendix the logarithmic part of the matching coefficients for lpTMDPDFs are collected. Note that these coefficients are not original, in the sense that they can be predicted from the NLO matching derived in [8, 21] via evolution equations as it is described in sec. 3.2. In our calculation we have derived these expressions directly, as part of the checks.

Recalling that the perturbative expansion of the coefficient function in eq. (2.10) is

$$\delta^L C_{g \leftarrow f}(x, \mathbf{b}; \mu, \zeta, \mu) = \sum_{n=1}^{\infty} a_s^n \delta^L C_{g \leftarrow f}^{[n]}(x, \mathbf{b}; \mu, \zeta, \mu), \quad (\text{B.1})$$

with $a_s = g^2/(4\pi)^2$ and solving the system of eq. (3.12, 3.13) we obtain

$$\delta^L C_{g \leftarrow f}^{[1]}(x, \mathbf{b}; \mu, \zeta, \mu) = \delta^L C_{g \leftarrow f}^{(1,0,0)}(x), \quad (\text{B.2})$$

$$\delta^L C_{g \leftarrow f}^{[2]}(x, \mathbf{b}; \mu, \zeta, \mu) = \left(-\frac{1}{2} \mathbf{L}_\mu^2 + \mathbf{L}_\mu \mathbf{l}_\zeta \right) \delta^L C_{g \leftarrow f}^{(2,1,1)}(x) + \mathbf{L}_\mu \delta^L C_{g \leftarrow f}^{(2,1,0)}(x) + \delta^L C_{g \leftarrow f}^{(2,0,0)}(x), \quad (\text{B.3})$$

where

$$\mathbf{L}_\mu = \ln \left(\frac{\mu^2 \mathbf{b}^2}{4e^{-\gamma_E}} \right), \quad \mathbf{l}_\zeta = \ln \left(\frac{\mu^2}{\zeta} \right). \quad (\text{B.4})$$

Using expression for the NLO coefficients (3.20,3.21) and the LO DGLAP kernels [58] and expressions for anomalous dimensions (see e.g.[20]) we obtain

$$\delta^L C_{g \leftarrow g}^{(2,1,1)}(x) = -8C_A^2 \frac{1-x}{x}, \quad (\text{B.5})$$

$$\begin{aligned} \delta^L C_{g \leftarrow g}^{(2;1,0)}(x) = & -16C_A^2 \left\{ \frac{1+x}{x} \ln x + \frac{1-x}{x} \left[\frac{x}{6}(2-x) + \frac{15}{4} - \ln(1-x) \right] \right\} \\ & + 16C_F T_r N_f \left[\frac{1}{3} \frac{1-x}{x} (2 + (2-x)x) + \ln x \right] + \frac{16}{3} C_A T_r N_f \frac{1-x}{x}, \end{aligned} \quad (\text{B.6})$$

$$\delta^L C_{g \leftarrow q}^{(2,1,1)}(x) = -8C_F C_A \frac{1-x}{x}, \quad (\text{B.7})$$

$$\begin{aligned} \delta^L C_{g \leftarrow q}^{(2;1,0)}(x) = & -4C_F C_A \left[\frac{1-x}{x} \left(\frac{43}{3} + x \right) + 4 \frac{1+x}{x} \ln x \right] \\ & + 4C_F^2 \left[\frac{1-x}{x} (x + 4 \ln(1-x)) + 2 \ln x \right] + \frac{32}{3} C_F T_r N_f \frac{1-x}{x}, \end{aligned} \quad (\text{B.8})$$

where $C_A = N_c$, $C_F = (N_c^2 - 1)/2N_c$ are Casimir eigenvalues of adjoint and fundamental representation for $SU(N_c)$ -gauge group, $T_r = 1/2$ is the normalization of Gell-Mann matrices, and N_f is the number of quark flavors.

References

- [1] J. R. Ellis, M. K. Gaillard and D. V. Nanopoulos, *A Phenomenological Profile of the Higgs Boson*, *Nucl. Phys.* **B106** (1976) 292.
- [2] M. Spira, A. Djouadi, D. Graudenz and P. M. Zerwas, *Higgs boson production at the LHC*, *Nucl. Phys.* **B453** (1995) 17–82, [[hep-ph/9504378](#)].
- [3] A. Djouadi, *The Anatomy of electro-weak symmetry breaking. I: The Higgs boson in the standard model*, *Phys. Rept.* **457** (2008) 1–216, [[hep-ph/0503172](#)].
- [4] J. Collins, *Foundations of perturbative QCD*. Cambridge University Press, 2013.
- [5] M. G. Echevarria, A. Idilbi and I. Scimemi, *Factorization Theorem For Drell-Yan At Low q_T And Transverse Momentum Distributions On-The-Light-Cone*, *JHEP* **07** (2012) 002, [[1111.4996](#)].
- [6] M. G. Echevarria, A. Idilbi and I. Scimemi, *Unified treatment of the QCD evolution of all (un-)polarized transverse momentum dependent functions: Collins function as a study case*, *Phys. Rev.* **D90** (2014) 014003, [[1402.0869](#)].
- [7] A. Vladimirov, *Structure of rapidity divergences in soft factors*, *JHEP* **04** (2018) 045, [[1707.07606](#)].
- [8] M. G. Echevarria, T. Kasemets, P. J. Mulders and C. Pisano, *QCD evolution of (un)polarized gluon TMDPDFs and the Higgs q_T -distribution*, *JHEP* **07** (2015) 158, [[1502.05354](#)].
- [9] S. Catani and M. Grazzini, *QCD transverse-momentum resummation in gluon fusion processes*, *Nucl. Phys.* **B845** (2011) 297–323, [[1011.3918](#)].
- [10] D. Boer, W. J. den Dunnen, C. Pisano, M. Schlegel and W. Vogelsang, *Linearly Polarized Gluons and the Higgs Transverse Momentum Distribution*, *Phys. Rev. Lett.* **108** (2012) 032002, [[1109.1444](#)].
- [11] T. Becher, M. Neubert and D. Wilhelm, *Higgs-Boson Production at Small Transverse Momentum*, *JHEP* **05** (2013) 110, [[1212.2621](#)].
- [12] P. J. Mulders and J. Rodrigues, *Transverse momentum dependence in gluon distribution and fragmentation functions*, *Phys. Rev.* **D63** (2001) 094021, [[hep-ph/0009343](#)].
- [13] T. Becher and M. Neubert, *Drell-Yan Production at Small q_T , Transverse Parton Distributions and the Collinear Anomaly*, *Eur. Phys. J.* **C71** (2011) 1665, [[1007.4005](#)].
- [14] G. Bozzi, S. Catani, D. de Florian and M. Grazzini, *Transverse-momentum resummation and the spectrum of the Higgs boson at the LHC*, *Nucl. Phys.* **B737** (2006) 73–120, [[hep-ph/0508068](#)].
- [15] S. Mantry and F. Petriello, *Factorization and Resummation of Higgs Boson Differential Distributions in Soft-Collinear Effective Theory*, *Phys. Rev.* **D81** (2010) 093007, [[0911.4135](#)].
- [16] D. de Florian, G. Ferrera, M. Grazzini and D. Tommasini, *Transverse-momentum resummation: Higgs boson production at the Tevatron and the LHC*, *JHEP* **11** (2011) 064, [[1109.2109](#)].
- [17] W. Bizoń, X. Chen, A. Gehrmann-De Ridder, T. Gehrmann, N. Glover, A. Huss et al., *Fiducial distributions in Higgs and Drell-Yan production at $N^3LL+NNLO$* , *JHEP* **12** (2018) 132, [[1805.05916](#)].
- [18] J. Cruz-Martinez, T. Gehrmann, E. W. N. Glover and A. Huss, *Second-order QCD effects in Higgs boson production through vector boson fusion*, *Phys. Lett.* **B781** (2018) 672–677, [[1802.02445](#)].
- [19] T. Gehrmann, T. Luebbert and L. L. Yang, *Calculation of the transverse parton distribution functions at next-to-next-to-leading order*, *JHEP* **06** (2014) 155, [[1403.6451](#)].
- [20] M. G. Echevarria, I. Scimemi and A. Vladimirov, *Unpolarized Transverse Momentum Dependent Parton Distribution and Fragmentation Functions at next-to-next-to-leading order*, *JHEP* **09** (2016) 004, [[1604.07869](#)].
- [21] D. Gutierrez-Reyes, I. Scimemi and A. A. Vladimirov, *Twist-2 matching of transverse momentum dependent distributions*, *Phys. Lett.* **B769** (2017) 84–89, [[1702.06558](#)].

- [22] I. Scimemi and A. Vladimirov, *Systematic analysis of double-scale evolution*, *JHEP* **08** (2018) 003, [[1803.11089](#)].
- [23] I. Scimemi and A. Vladimirov, *Analysis of vector boson production within TMD factorization*, *Eur. Phys. J. C* **78** (2018) 89, [[1706.01473](#)].
- [24] V. Bertone, I. Scimemi and A. Vladimirov, *Extraction of unpolarized quark transverse momentum dependent parton distributions from Drell-Yan/Z-boson production*, *JHEP* **06** (2019) 028, [[1902.08474](#)].
- [25] X. Chen, T. Gehrmann, E. W. N. Glover, A. Huss, Y. Li, D. Neill et al., *Precise QCD Description of the Higgs Boson Transverse Momentum Spectrum*, *Phys. Lett. B* **788** (2019) 425–430, [[1805.00736](#)].
- [26] M. G. Echevarria, I. Scimemi and A. Vladimirov, *Transverse momentum dependent fragmentation function at next-to-next-to leading order*, *Phys. Rev. D* **93** (2016) 011502, [[1509.06392](#)].
- [27] M. G. Echevarria, I. Scimemi and A. Vladimirov, *Universal transverse momentum dependent soft function at NNLO*, *Phys. Rev. D* **93** (2016) 054004, [[1511.05590](#)].
- [28] D. Gutierrez-Reyes, I. Scimemi and A. Vladimirov, *Transverse momentum dependent transversely polarized distributions at next-to-next-to-leading-order*, *JHEP* **07** (2018) 172, [[1805.07243](#)].
- [29] D. Boer, S. J. Brodsky, P. J. Mulders and C. Pisano, *Direct Probes of Linearly Polarized Gluons inside Unpolarized Hadrons*, *Phys. Rev. Lett.* **106** (2011) 132001, [[1011.4225](#)].
- [30] A. Metz and J. Zhou, *Distribution of linearly polarized gluons inside a large nucleus*, *Phys. Rev. D* **84** (2011) 051503, [[1105.1991](#)].
- [31] F. Dominguez, J.-W. Qiu, B.-W. Xiao and F. Yuan, *On the linearly polarized gluon distributions in the color dipole model*, *Phys. Rev. D* **85** (2012) 045003, [[1109.6293](#)].
- [32] C. Pisano, D. Boer, S. J. Brodsky, M. G. A. Buffing and P. J. Mulders, *Linear polarization of gluons and photons in unpolarized collider experiments*, *JHEP* **10** (2013) 024, [[1307.3417](#)].
- [33] A. Dumitru, T. Lappi and V. Skokov, *Distribution of Linearly Polarized Gluons and Elliptic Azimuthal Anisotropy in Deep Inelastic Scattering Dijet Production at High Energy*, *Phys. Rev. Lett.* **115** (2015) 252301, [[1508.04438](#)].
- [34] A. Mukherjee and S. Rajesh, *Linearly polarized gluons in charmonium and bottomonium production in color octet model*, *Phys. Rev. D* **95** (2017) 034039, [[1611.05974](#)].
- [35] D. Boer, P. J. Mulders, J. Zhou and Y.-j. Zhou, *Suppression of maximal linear gluon polarization in angular asymmetries*, *JHEP* **10** (2017) 196, [[1702.08195](#)].
- [36] A. V. Efremov, N. Ya. Ivanov and O. V. Teryaev, *How to measure the linear polarization of gluons in unpolarized proton using the heavy-quark pair leptonproduction*, *Phys. Lett. B* **777** (2018) 435–441, [[1711.05221](#)].
- [37] A. V. Efremov, N. Y. Ivanov and O. V. Teryaev, *The ratio $R = d\sigma_L/d\sigma_T$ in heavy-quark pair leptonproduction as a probe of linearly polarized gluons in unpolarized proton*, *Phys. Lett. B* **780** (2018) 303–307, [[1801.03398](#)].
- [38] R. Kishore and A. Mukherjee, *Accessing linearly polarized gluon distribution in J/ψ production at the electron-ion collider*, *Phys. Rev. D* **99** (2019) 054012, [[1811.07495](#)].
- [39] L. D. McLerran and R. Venugopalan, *Gluon distribution functions for very large nuclei at small transverse momentum*, *Phys. Rev. D* **49** (1994) 3352–3355, [[hep-ph/9311205](#)].
- [40] “artemide web-page, <https://teorica.fis.ucm.es/artemide/> artemide repository, <https://github.com/vladimirovalexy/artemide-public>.”
- [41] I. Scimemi, A. Tarasov and A. Vladimirov, *Collinear matching for Sivers function at next-to-leading order*, *JHEP* **05** (2019) 125, [[1901.04519](#)].

- [42] T. Gehrmann, T. Lubbert and L. L. Yang, *Transverse parton distribution functions at next-to-next-to-leading order: the quark-to-quark case*, *Phys. Rev. Lett.* **109** (2012) 242003, [[1209.0682](#)].
- [43] M. G. Echevarria, A. Idilbi and I. Scimemi, *Soft and Collinear Factorization and Transverse Momentum Dependent Parton Distribution Functions*, *Phys. Lett.* **B726** (2013) 795–801, [[1211.1947](#)].
- [44] S. Moch, J. A. M. Vermaseren and A. Vogt, *The Quark form-factor at higher orders*, *JHEP* **08** (2005) 049, [[hep-ph/0507039](#)].
- [45] T. Gehrmann, E. W. N. Glover, T. Huber, N. Ikizlerli and C. Studerus, *Calculation of the quark and gluon form factors to three loops in QCD*, *JHEP* **06** (2010) 094, [[1004.3653](#)].
- [46] A. A. Vladimirov, *Soft-/rapidity- anomalous dimensions correspondence*, *Phys. Rev. Lett.* **118** (2017) 062001, [[1610.05791](#)].
- [47] Y. Li and H. X. Zhu, *Bootstrapping Rapidity Anomalous Dimensions for Transverse-Momentum Resummation*, *Phys. Rev. Lett.* **118** (2017) 022004, [[1604.01404](#)].
- [48] J. C. Collins and D. E. Soper, *Back-To-Back Jets: Fourier Transform from B to K-Transverse*, *Nucl. Phys.* **B197** (1982) 446–476.
- [49] I. Scimemi and A. Vladimirov, *Power corrections and renormalons in Transverse Momentum Distributions*, *JHEP* **03** (2017) 002, [[1609.06047](#)].
- [50] M. A. Shifman, A. I. Vainshtein, M. B. Voloshin and V. I. Zakharov, *Low-Energy Theorems for Higgs Boson Couplings to Photons*, *Sov. J. Nucl. Phys.* **30** (1979) 711–716.
- [51] M. Kramer, E. Laenen and M. Spira, *Soft gluon radiation in Higgs boson production at the LHC*, *Nucl. Phys.* **B511** (1998) 523–549, [[hep-ph/9611272](#)].
- [52] K. G. Chetyrkin, B. A. Kniehl and M. Steinhauser, *Hadronic Higgs decay to order α_s^{**4}* , *Phys. Rev. Lett.* **79** (1997) 353–356, [[hep-ph/9705240](#)].
- [53] V. Ahrens, T. Becher, M. Neubert and L. L. Yang, *Renormalization-Group Improved Prediction for Higgs Production at Hadron Colliders*, *Eur. Phys. J.* **C62** (2009) 333–353, [[0809.4283](#)].
- [54] V. Ahrens, T. Becher, M. Neubert and L. L. Yang, *Origin of the Large Perturbative Corrections to Higgs Production at Hadron Colliders*, *Phys. Rev.* **D79** (2009) 033013, [[0808.3008](#)].
- [55] CMS collaboration, V. Khachatryan et al., *Measurement of differential cross sections for Higgs boson production in the diphoton decay channel in pp collisions at $\sqrt{s} = 8$ TeV*, *Eur. Phys. J.* **C76** (2016) 13, [[1508.07819](#)].
- [56] NNPDF collaboration, R. D. Ball et al., *Parton distributions from high-precision collider data*, *Eur. Phys. J.* **C77** (2017) 663, [[1706.00428](#)].
- [57] V. A. Smirnov, *Evaluating Feynman integrals*, *Springer Tracts Mod. Phys.* **211** (2004) 1–244.
- [58] G. Altarelli and G. Parisi, *Asymptotic Freedom in Parton Language*, *Nucl. Phys.* **B126** (1977) 298–318.